Data-driven approach to pressure determination in valves and arteries

H. Švihlová[a], J. Hron[a], J. Málek[a], K. R. Rajagopal[b] and K. Rajagopal[c]

a, Mathematical Institute, Charles University, Czech Republic

b, Texas A&M University, College Station TX, United States

c, Memorial Hermann Texas Medical Center, Houston TX, United States

CIVIL-COMP-OPTI, Riva del Garda, September 16, 2019

The presentation is based on the following study:

H. Švihlová, J. Hron, J. Málek, K. R. Rajagopal, K. Rajagopal (2016): *Determination of pressure data from velocity data with a view toward its application in cardiovascular mechanics. Part 1. Theoretical considerations*. In: International Journal of Engineering Science 105,108–127.

H. Švihlová, J. Hron, J. Málek, K. R. Rajagopal, K. Rajagopal (2017): *Determination of pressure data from velocity data with a view towards its application in cardiovascular mechanics. Part 2: A study of aortic valve stenosis*. In: International Journal of Engineering Science 114,1–15.

The work was supported by AZV CR grant no. 17-32872A "Correlation of modelling hemodynamic parameters with histological changes in the wall of cerebral aneurysms" and no. NV19-04-00270 "Assessment of hemodynamic parameters of stable and unstable atherosclerotic plaques in the carotid arteries in in vitro models."

Motivation

Current medical methods in stenosis evaluation and pressure determination

Pressure determination - continuum mechanics approach

Pressure difference and energy dissipation dependence on the stenosis severity

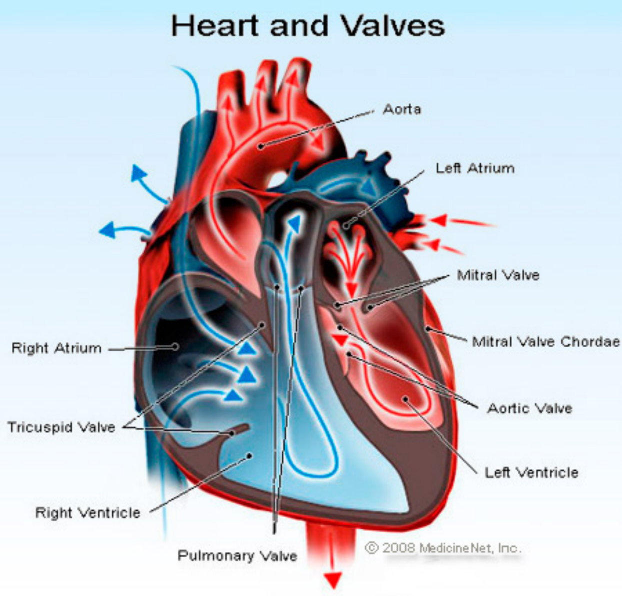
Heart and Valves
Aorta
Left Atrium
Mitral Valve
Mitral Valve Chordae
Right Atrium
Aortic Valve
Tricuspid Valve
Left Ventricle
Right Ventricle
Pulmonary Valve
© 2008 MedicineNet, Inc.

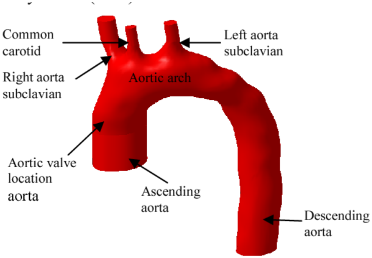

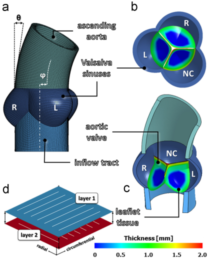

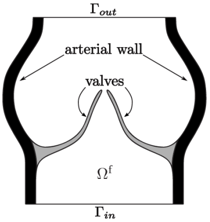

A. A. Basri et al.: Computational fluid dynamics study of the aortic valve opening on hemodynamics characteristics. In: 2014 IEEE Conference on Biomedical Engineering and Sciences (IECBES) (2014):99–102.

F. Sturla et al.: Impact of different aortic valve calcification patterns on the outcome of transcatheter aortic valve implantation: A finite element study. In: Journal of Biomechanics 49.12 (2016):2520–2530.

S. C. Shadden, M. Astorino and J-F. Gerbeau: Computational analysis of an aortic valve jet with Lagrangian coherent structures. In: Chaos: An Interdisciplinary Journal of Nonlinear Science 20.1 (2010):017512.

Motivation

Current medical methods in stenosis evaluation and pressure determination

Pressure determination - continuum mechanics approach

Pressure difference and energy dissipation dependence on the stenosis severity

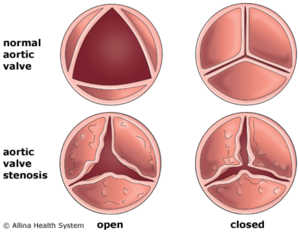

- anatomic stenosis

$$severity = \left(1 - \frac{area_{stenotic}}{area_{healthy}}\right) \cdot 100\%$$

- physiologically important stenosis
  - valve area/effective orifice area
  - additional heart work/energy dissipation
  - trans-stenosis pressure difference

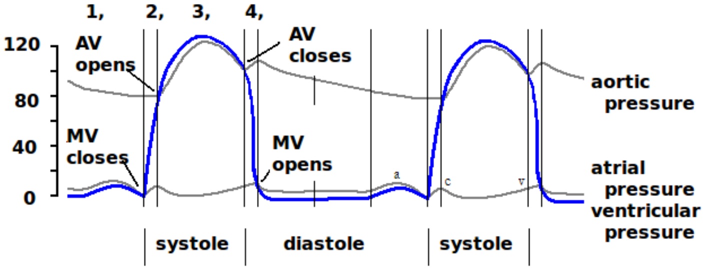

Figure: **Blood pressure in the left ventricle during a cardiac cycle.** (from Wikipedia, modified.)

Phase 1, diastolic filling

Phase 2, isovolumic contraction

Phase 3, systolic ejection

Phase 4, isovolumic relaxation

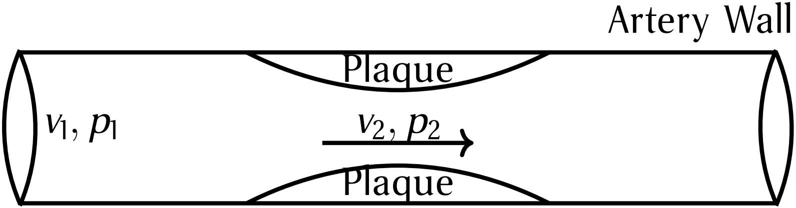

$$\frac{1}{2}\rho_* v_1^2 + h_1 \rho_* g_* = \frac{1}{2}\rho_* v_2^2 + h_2 \rho_* g$$

$$(h_1 - h_2)\rho_* g_* = \frac{1}{2}\rho_* v_2^2$$

$$(h_1 - h_2) = C v_2^2$$

H. Baumgartner et al.: Echocardiographic assessment of valve stenosis: EAE/ASE recommendations for clinical practice. In: European Journal of Echocardiography, 10(1) (2009): 1–25.

Motivation

Current medical methods in stenosis evaluation and pressure determination

Pressure determination - continuum mechanics approach

Pressure difference and energy dissipation dependence on the stenosis severity

$$\nabla p = -\rho_* \left((\nabla \mathbf{v})\, \mathbf{v} - \frac{\partial \mathbf{v}}{\partial t} \right) + \operatorname{div}(2\mu_* \mathbf{D}) =: \mathbf{f}$$

$$\begin{aligned} -\Delta q_{\text{ppe}} &= \operatorname{div} \mathbf{f} && \text{in } \Omega \\ \frac{\partial q_{\text{ppe}}}{\partial \mathbf{n}} &= \mathbf{n} \cdot \mathbf{f} && \text{on } \partial\Omega \\ q_{\text{ppe}} &= p_* && \text{on } \Gamma_{out} \end{aligned}$$

$$\nabla p = -\rho_* \left((\nabla \mathbf{v})\, \mathbf{v} - \frac{\partial \mathbf{v}}{\partial t} \right) + \operatorname{div}(2\mu_* \mathbf{D}) =: \mathbf{f}$$

$$\begin{aligned}
-\Delta \mathbf{a} + \nabla q_{\text{ste}} &= \mathbf{f} && \text{in } \Omega,\\
\operatorname{div} \mathbf{a} &= 0 && \text{in } \Omega,\\
\mathbf{a} &= 0 && \text{on } \partial\Omega,\\
q_{\text{ste}} &= p_* && \text{on } \Gamma_{out}.
\end{aligned}$$

M. E. Cayco and R. A. Nicolaides: Finite Element Technique for Optimal Pressure Recovery from Stream Function Formulation of Viscous Flows. In: Mathematics of Computation, 46.174 (1986): 371–377.

- time resolved phase-contrast magnetic resonance imaging 4D-PCMR (4D Flow MRI)
- limitations in both spatial and temporal resolution of the signals

A. Bakhshinejad et al.: Merging Computational Fluid Dynamics and 4D Flow MRI Using Proper Orthogonal Decomposition and Ridge Regression. In: Journal of Biomechanics 58 (2017): 162–173.

V. C. Rispoli et al.: Computational fluid dynamics simulations of blood flow regularized by 3D phase contrast MRI. In: BioMedical Engineering OnLine 14.1 (2015).

- fixing pressure (catheterization)

incompressible unstationary Navier-Stokes equation, no-slip wall, velocity prescribed on the inlet with parabolic profile, pressure and the backflow stabilization/penalization prescribed on the outlet

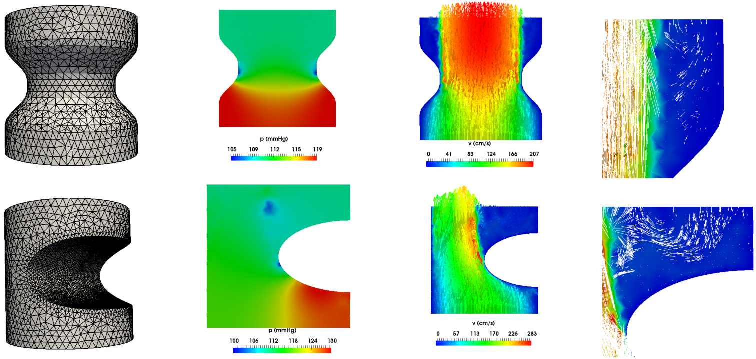

	$\frac{\|q_{\text{ppe}} - p_{ref}\|_{L^2}}{\|p_{ref}\|_{L^2}}$	$\frac{\|q_{\text{ste}} - p_{ref}\|_{L^2}}{\|p_{ref}\|_{L^2}}$
symmetric	6.40e-04	1.50e-14
non-symmetric	3.50e-03	1.16e-14

Table: Relative errors for fine data.

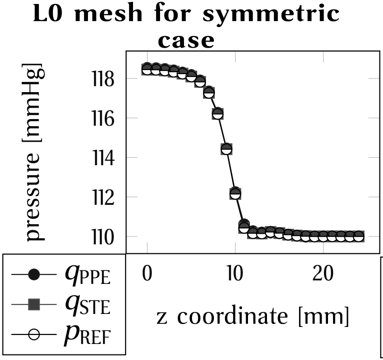

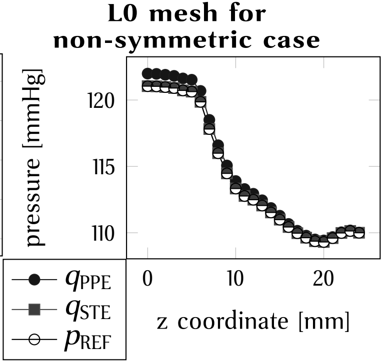

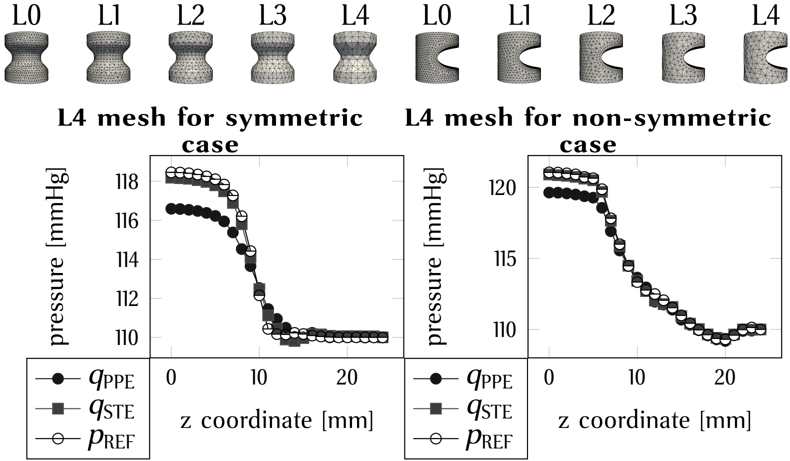

L0
L1
L2
L3
L4
L0
L1
L2
L3
L4
L4 mesh for symmetric case
L4 mesh for non-symmetric case
pressure [mmHg]
118
116
114
112
110
z coordinate [mm]
0
10
20
q_{PPE}
q_{STE}
p_{REF}
pressure [mmHg]
120
115
110
z coordinate [mm]
0
10
20
q_{PPE}
q_{STE}
p_{REF}

	symmetric case			non-symmetric case		
	err_{ppe}	err_{ste}	$\frac{err_{ppe}}{err_{ste}}$	err_{ppe}	err_{ste}	$\frac{err_{ppe}}{err_{ste}}$
L0N0	6.40e-04	1.50e-14	4.27e10	3.50e-03	1.16e-14	3.02e11
L1N0	1.49e-03	1.03e-03	1.44	2.53e-03	1.68e-03	1.51
L2N0	2.24e-03	1.46e-03	1.54	3.33e-03	2.20e-03	1.51
L3N0	6.52e-03	2.15e-03	3.04	5.82e-03	3.05e-03	1.91
L4N0	9.37e-03	3.14e-03	2.99	8.46e-03	4.05e-03	2.09

Table: Relative errors for PPE and STE methods.

$$err_{ppe} = \frac{\|q_{ppe} - p_{ref}\|_{L^2}}{\|p_{ref}\|_{L^2}}, \; err_{ste} = \frac{\|q_{ste} - p_{ref}\|_{L^2}}{\|p_{ref}\|_{L^2}}$$

- two sources of error in velocity field:
  - interpolation error due to the limited amount of points with known velocity
  - velocity vectors are measured with the error/noise
- to simulate the latter one, we add a random number $\varepsilon \in [-0.05, 0.05]$, $\varepsilon \in [-0.1, 0.1]$ respectively, to each point where we know the velocity
- $\mathbf{v}_{\text{exact}}(\overline{\mathbf{x}}) \approx \mathbf{v}_{\text{meas}}(\overline{\mathbf{x}}) = (1 \pm \varepsilon(\overline{\mathbf{x}}))\mathbf{v}_{\text{exact}}(\overline{\mathbf{x}})$
  - $\varepsilon(\overline{\mathbf{x}}) \in [0, 0.05]$ for maximal 5% error
  - $\varepsilon(\overline{\mathbf{x}}) \in [0, 0.1]$ for maximal 10% error

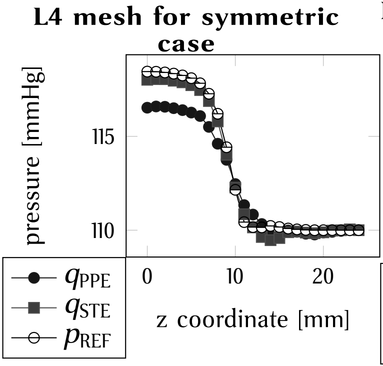

L4 mesh for symmetric case
pressure [mmHg]
115
110
0
10
20
z coordinate [mm]
q_{PPE}
q_{STE}
p_{REF}

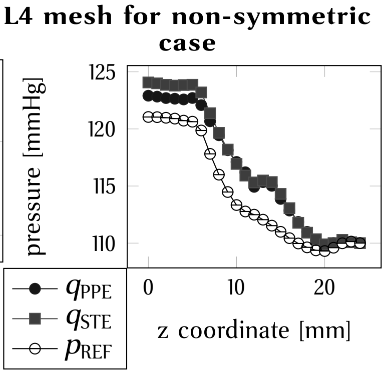

L4 mesh for non-symmetric case
pressure [mmHg]
125
120
115
110
0
10
20
z coordinate [mm]
q_{PPE}
q_{STE}
p_{REF}

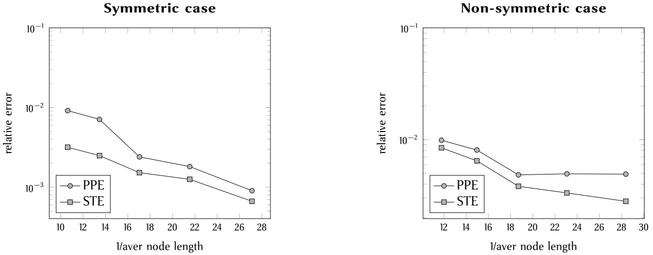

Convergence curves of relative errors for coarse data with 5% noise.

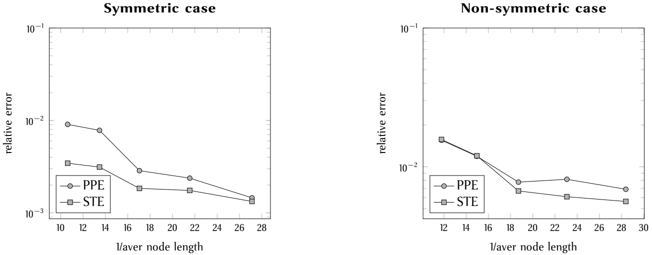

Convergence curves of relative errors for coarse data with 10% noise.

PPE

- poisson equation
- additional derivative of the data vector $\mathbf{f}(\mathbf{v})$
- underestimate the pressure difference
- fixing p at the outlet
- limiting accuracy with noisy velocity fields

STE

- larger linear problem
- less regularity requirements on the data (velocity field)
- better approximation $\|q_{\text{ste}} - p\|_{L^2}$
- fixing p at the outlet
- limiting accuracy with noisy velocity fields

Motivation

Current medical methods in stenosis evaluation and pressure determination

Pressure determination - continuum mechanics approach

Pressure difference and energy dissipation dependence on the stenosis severity

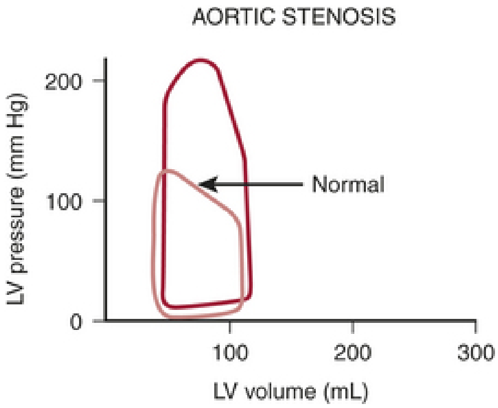

clinicalgate.com

C. W. Akins, B. Travis, A. P. Yoganathan: Energy loss for evaluating heart valve performance. (2008) In: The Journal of Thoracic and Cardiovascular Surgery 136.4,820–833.

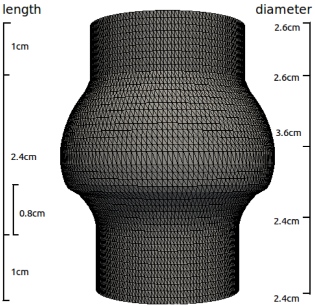

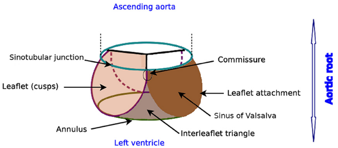

J. H. Spühler et al.: 3D Fluid-Structure Interaction Simulation of Aortic Valves Using a Unified Continuum ALE FEM Model. In: Frontiers in Physiology 9 (2018).

The parts of the geometry (from below): left ventricular outflow tract, ventriculo-aortic junction, aortic root (the first third should be stenotic), sinotubular junction, ascending aorta.

$$
\begin{aligned}
\rho_* \left(\frac{\partial \mathbf{v}}{\partial t} + (\nabla \mathbf{v})\, \mathbf{v} \right) - \operatorname{div}\left(2\mu_* \mathbf{D}(\mathbf{v})\right) + \nabla p &= \mathbf{0} && \text{in } \Omega, \\
\operatorname{div} \mathbf{v} &= 0 && \text{in } \Omega, \\
\mathbf{T} &= -p\mathbf{I} + 2\mu_* \mathbf{D} && \text{in } \Omega, \\
\mathbf{v} &= \mathbf{0} && \text{on } \Gamma_{wall}, \\
\mathbf{v} &= \mathbf{v}_{in} && \text{on } \Gamma_{in}, \\
\mathbf{T}\mathbf{n} - \frac{1}{2}\rho_* (\mathbf{v} \cdot \mathbf{n})_- \mathbf{v} &= -\overline{P(t)}\mathbf{n} && \text{on } \Gamma_{out}.
\end{aligned}
$$

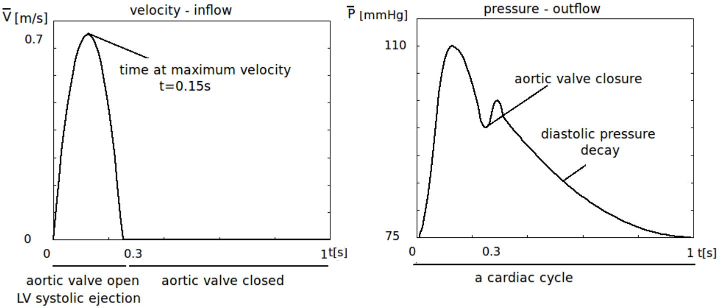

Inflow velocity magnitude $\overline{V(t)}$ and outlet pressure $\overline{P(t)}$ as functions of time.

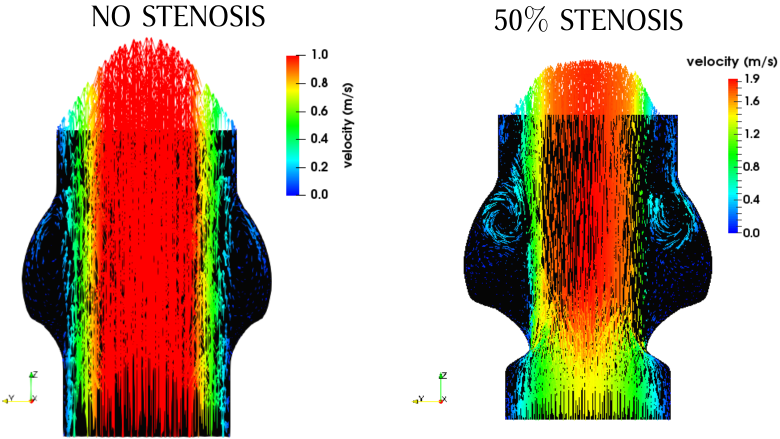

NO STENOSIS
1.0
0.8
0.6
0.4
0.2
0.0
velocity (m/s)
Z
Y
X
50% STENOSIS
velocity (m/s)
1.9
1.6
1.2
0.8
0.4
0.0
Z
Y
X

$$p = \frac{\int_{\Gamma_z} p \, dS}{\text{area}(\Gamma_z)}$$

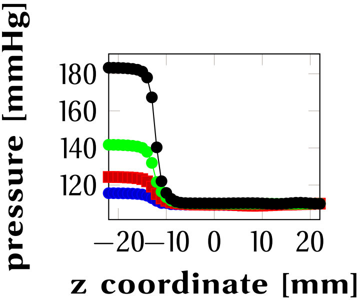

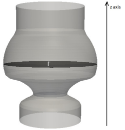

$$E_{dis} = \frac{\int_{\Gamma_z} \mathbf{T} : \mathbf{D} \, dS}{\text{area}(\Gamma_z)}$$

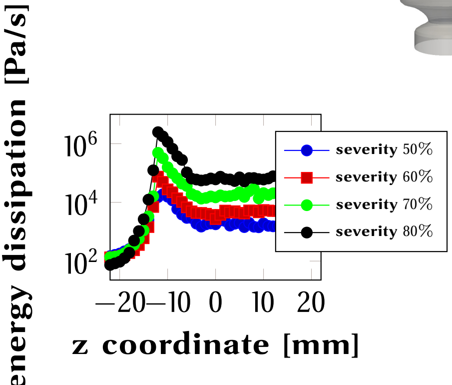

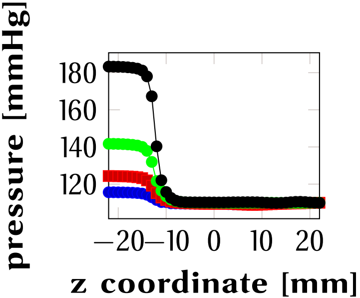

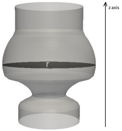

sev	NS $p_1 - p_2$ [mmHg]	SB $p_1 - p_2$ [mmHg]
50%	5.6	7.8
60%	14.3	12.3
70%	31.7	21.8
80%	73.3	49

Table: Maximal pressure difference computed through the Navier-Stokes eq. and simplified Bernoulli eq.

- the current methods for stenosis evaluation (whether this is physiologically important or not) are based on pressure difference computed through the simplified Bernoulli equation (pressure difference proportional to v^2)
- continuum mechanics models are available to determine the pressure from the velocity field
- presented method, leading to the Stokes equation, allow us to compute the pressure under lower regularity requirements on the given velocity and it was shown that it provides more accurate pressure approximation
- the pressure and energy dissipation were computed in the geometries with narrowing up to 80% - knowing the velocity field at the inlet (the left ventricular outflow) and pressure at the outlet (the ascending aorta)

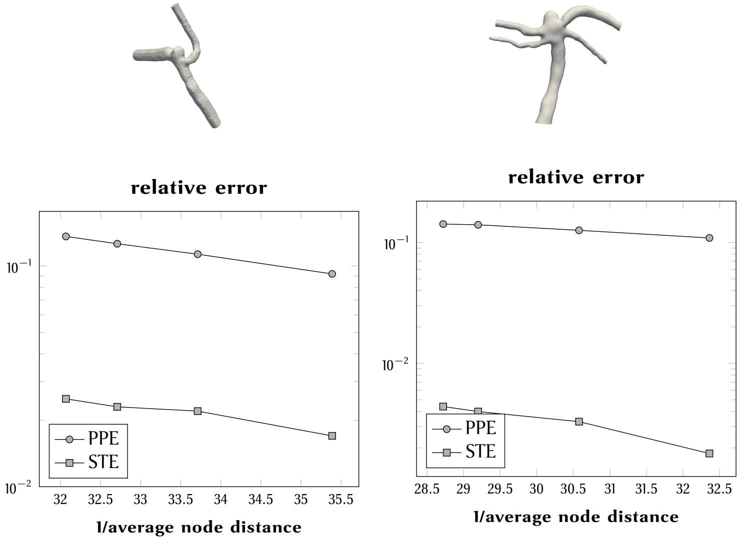
relative error
PPE
STE
10^{-1}
10^{-2}
32
32.5
33
33.5
34
34.5
35
35.5
1/average node distance
relative error
PPE
STE
10^{-1}
10^{-2}
28.5
29
29.5
30
30.5
31
31.5
32
32.5
1/average node distance

NOSLIP

$$\mathbf{v} \cdot \mathbf{n} = 0$$
$$\mathbf{v} \cdot \tau = 0$$

NAVIER SLIP K=0.5

$$\mathbf{v} \cdot \mathbf{n} = 0$$
$$\mathbf{Tn} \cdot \tau = -\frac{1}{K}\mathbf{v} \cdot \tau$$

PERFECT-SLIP

$$\mathbf{v} \cdot \mathbf{n} = 0$$
$$\mathbf{Tn} \cdot \tau = \mathbf{0}$$

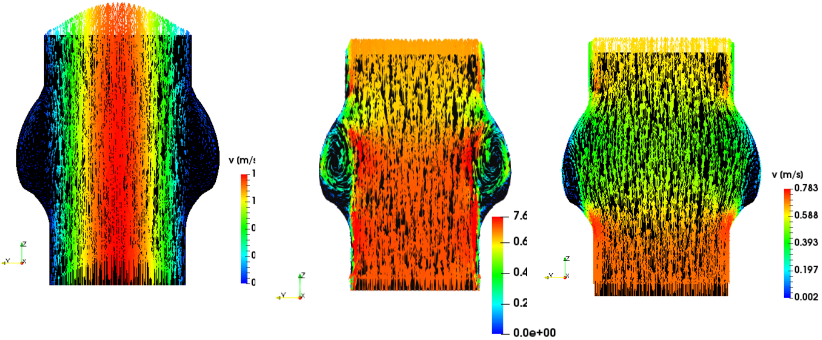

Figure: Velocity distribution on a slice of the valvular geometry without severity in time of maximal velocity ($t = 0.15\,\mathrm{s}$): all plug-in profiles.

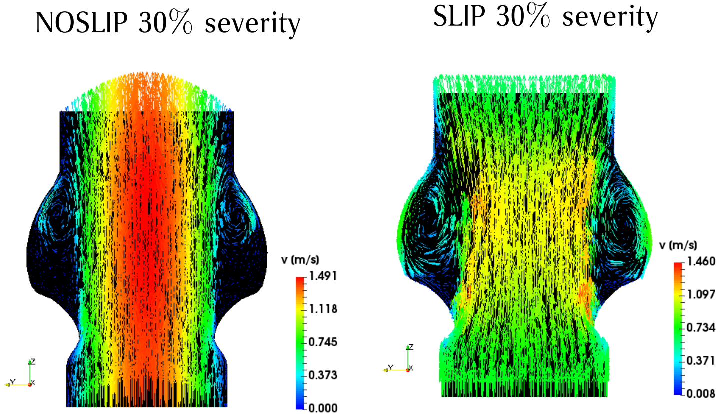

Figure: Velocity distribution on a slice of the valvular geometry with 30% severity in time of maximal velocity ($t = 0.15\,\mathrm{s}$).

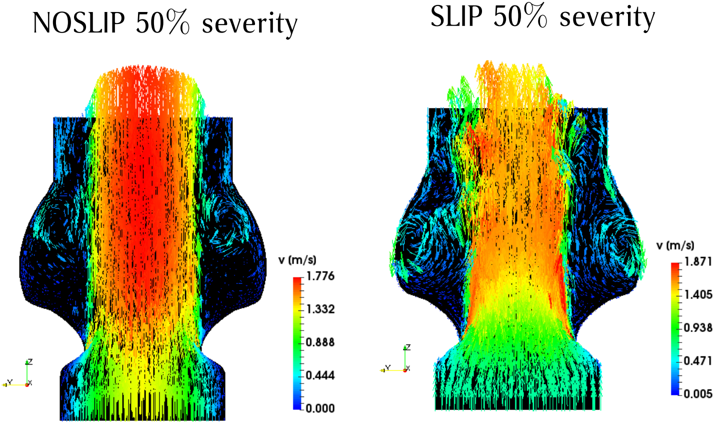

Figure: Velocity distribution on a slice of the valvular geometry with 50% severity in time of maximal velocity ($t = 0.15\,\mathrm{s}$).

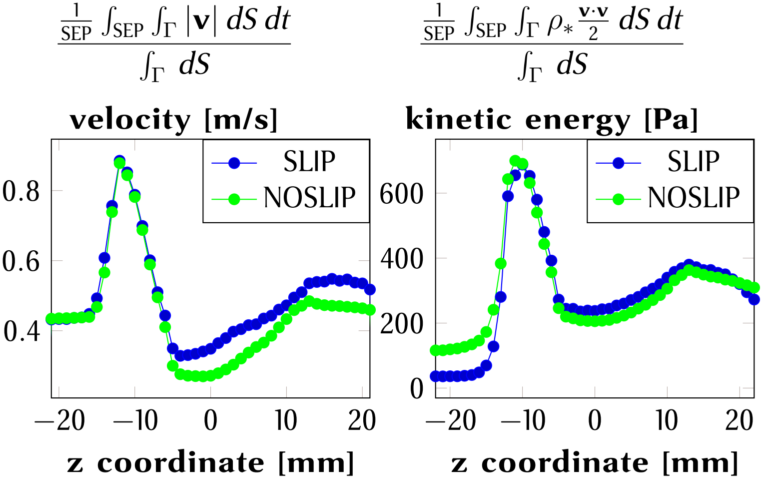

50% STENOSIS, time-averaged values (over SEP)

$$\frac{\frac{1}{\mathrm{SEP}}\int_{\mathrm{SEP}}\int_{\Gamma} p\, dS\, dt}{\int_{\Gamma}\, dS}$$

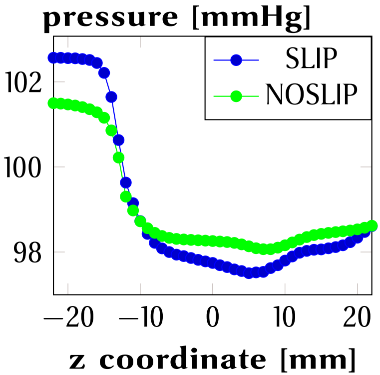

$$\frac{\frac{1}{\mathrm{SEP}}\int_{\mathrm{SEP}}\int_{\Gamma} 2\mu_{*}\mathbf{D}{:}\mathbf{D}\, dS\, dt}{\int_{\Gamma}\, dS}$$

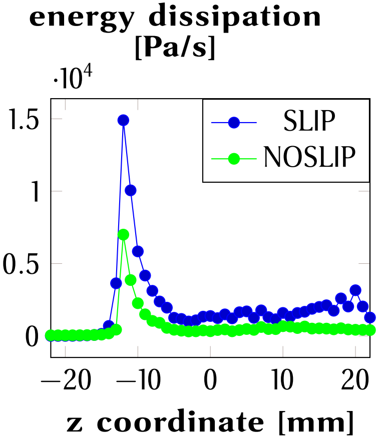

50% STENOSIS, time-averaged values (over SEP)

Thank you for your attention.